Journal of Mathematical Research with Applications
May, 2013, Vol. 33, No. 3, pp. 253–272
DOI:10.3770/j.issn:2095-2651.2013.03.001
Http://jmre.dlut.edu.cn

On a Variational Model for Selective Image Segmentation of Features with Infinite Perimeter

Lavdie RADA, Ke CHEN*
Centre for Mathematical Imaging Techniques and Department of Mathematical Sciences, University of Liverpool, Liverpool L69 7ZL, United Kingdom

Abstract Variational models provide reliable formulation for segmentation of features and their boundaries in an image, following the seminal work of Mumford-Shah (1989, Commun. Pure Appl. Math.) on dividing a general surface into piecewise smooth sub-surfaces. A central idea of models based on this work is to minimize the length of feature's boundaries (i.e., $\mathcal{H}^1$ Hausdorff measure). However there exist problems with irregular and oscillatory object boundaries, where minimizing such a length is not appropriate, as noted by Barchiesi et al. (2010, SIAM J. Multiscale Model. Simu.) who proposed to miminize $\mathcal{L}^2$ Lebesgue measure of the γ-neighborhood of the boundaries. This paper presents a dual level set selective segmentation model based on Barchiesi et al. (2010) to automatically select a local feature instead of all global features. Our model uses two level set functions: a global level set which segments all boundaries, and the local level set which evolves and finds the boundary of the object closest to the geometric constraints. Using real life images with oscillatory boundaries, we show qualitative results demonstrating the effectiveness of the proposed method.

Keywords image selective segmentation; level set; edge detection; 2D image segmentation.

MR(2010) Subject Classification 62H35; 65N22; 68U10; 35A15; 65C20; 74G65; 74G75

1. Introduction

In the literature, a large variety of models and algorithms has been extensively proposed and successfully applied to image segmentation, which is a process of extracting the boundaries from a given image. Variational techniques [8, 27, 30] prove to be very efficient for extracting homogenous areas and segmenting a given image compared with other models such as statistical methods [12, 13, 42] or wavelet techniques [16, 24, 35].

The idea of boundary detection by minimizing a functional of a piecewise smooth representation of the image, introduced by Mumford and Shah [27], is widely adopted and used in different variational frameworks such as [1, 4, 6–8, 10, 11, 14, 20]. Among the variety of techniques including region growing [1, 44], edge detection and active contours [9, 17], image thresholding [22, 33] etc., the active contour has several advantages in that it is very easy and straightforward to implement, implicitly includes the computation of curvatures, and has a parameter that controls the smoothness of the results. Active contour methods can be classified as edge-based

Received April 5, 2012; Accepted February 19, 2013
* Corresponding author
E-mail address: cmit@liv.ac.uk (Lavdie RADA); k.chen@liv.ac.uk (Ke CHEN)

[6, 17, 23, 31, 36, 43] and region based models [9, 19, 20, 34]. Edge-based models are helped by the image gradient to stop the contour on the boundaries of the desired object while region-based methods utilize the image statistical information to construct constrains. Region-based methods are successful in cases of weak boundaries or even without boundaries. Variational level-set based segmentation methods distinguish all objects in an image foreground from its background. Such tasks, still remaining challenging for multiphases [37], have been deeply investigated by many researchers. In operational applications requiring selection such as medical imaging of a particular organ or CCTV monitoring of a subject, the commonly known models are not capable of doing such a selection task. The main challenge in a selective image segmentation problem is how to differentiate one feature from another similar (or nearby) feature or to avoid selecting spurious features. This challenging task of selecting one feature/object among the others leads to a new and challenging task of selective segmentation, which will be extracting a single object.

Recently several works have been proposed for the 2D selective segmentation based on active contours method [3, 15, 25, 32], which for a proper incorporation of some geometric priors information (markers) into the image processing by the user and edge detection technique, could lead to a good convergence to the target object. However, these models do not work in cases where the image has oscillatory boundaries since all techniques based on the weighted penalization term of the length, can give rise to some difficulties.

In this paper, we make use of $\mathcal{L}^2$ Lebesgue measure of the γ-neighborhood of the contour [5] as penalization term instead of the $\mathcal{H}^1$ Hausdorff measure and propose a local selective segmentation model, enabling to extract features with irregular and oscillatory boundaries.

The remainder of this paper is organized as follows. In Section 2, we describe some methods such as the classic Chan-Vese model [8], Barchiesi et al. [5] model, and the Dual Level-set Selective Segmentation (DLSS) model by Rada-Chen [32]. A new dual level-set selective model, which uses the $\mathcal{L}^2$ Lebesgue measure of the γ-neighborhood of the contour as penalization term, is presented in Section 3. A time marching and additive operator splitting (AOS) technique is developed for the numerical solution. In Section 4 the experimental results are presented based on artificial and real images. Conclusions are drawn in Section 5.

2. Review of some global active contours models and the local selection model of Rada-Chen [32]

The segmentation model by Mumford-Shah [26, 27] solves, given an image $u_0 = u_0(x, y)$,

$$\min_{u,\Gamma} F_{MS}(u, \Gamma) = \alpha \int_{\Omega\setminus\Gamma} |\nabla u|^2 \mathrm{d}x\mathrm{d}y + \mathcal{H}^{n-1}(\Gamma) + \lambda \int_{\Omega} (u - u_0)^2 \mathrm{d}x\mathrm{d}y \tag{1}$$

for the reconstruction u and the feature boundary set Γ, where Ω is a bounded subset of R^n with Lipschitz boundary, the ideal image $u(x, y)$ belonging to the space BV (Ω) the functions of bounded variation on (Ω), ∇u is the approximate gradient of $u(x, y)$, $\Gamma \in \Omega$ denotes the edge set of the image $u(x, y)$ which is the set of essential discontinuity points of $u(x, y)$, $\mathcal{H}^{n-1}$ is the $n - 1$ dimensional Hausdorff measure, which in the 2-dimensional case $\mathcal{H}^1$ denotes the length of the curve.

2.1 The Chan-Vese model [8]

Since the main difficulty in the study of the Mumford-Shah functional $F_{MS}(u,\Gamma)$ is the presence of the term $\mathcal{H}^{n-1}$, a natural way to approximate $F_{MS}(u,\Gamma)$ was introduced by Chan-Vese [8], which implemented the piecewise segmentation

$$\begin{aligned} &F_{cv}^{2D}(\Gamma,c_1,c_2)\\ &\quad=\mathcal{H}^1(\Gamma)+\lambda_{1cv}\int_{\text{inside}(\Gamma)}|u_0(x,y)-c_1|^2\mathrm{d}x\mathrm{d}y+\lambda_{2cv}\int_{\text{outside}(\Gamma)}|u_0(x,y)-c_2|^2\mathrm{d}x\mathrm{d}y \end{aligned} \tag{2}$$

where c_1 and c_2 are the average of $u_0(x,y)$ inside and outside (Γ), respectively. The unknown curve Γ can be represented by the zero level set of Lipschitz function $\phi:\Omega\to\mathbb{R}$

$$\begin{cases} \Gamma=\partial\Omega_1=\{(x,y)\in\Omega\;\big|\;\phi(x,y)=0\},\\ \text{inside}(\Gamma)=\Omega_1=\{(x,y)\in\Omega\;\big|\;\phi(x,y)>0\},\\ \text{outside}(\Gamma)=\Omega_2=\{(x,y)\in\Omega\;\big|\;\phi(x,y)<0\}, \end{cases}$$

and we rewrite the energy function in the form:

$$\begin{aligned} F(\phi,c_1,c_2)=&\mu_{cv}\int_\Omega|\nabla H(\phi)|\mathrm{d}x\mathrm{d}y+\lambda_{1cv}\int_\Omega|u_0(x,y)-c_1|^2H(\phi(x,y))\mathrm{d}x\mathrm{d}y+\\ &\lambda_{2cv}\int_\Omega|u_0(x,y)-c_2|^2(1-H(\phi(x,y)))\mathrm{d}x\mathrm{d}y, \end{aligned} \tag{3}$$

where H defines the Heaviside function

$$H(x)=\begin{cases}1 & \text{if } x\geq 0\\ 0 & \text{if } x<0.\end{cases}$$

2.2 The Barchiesi et al. model [5]

Following a variational framework, attempting to segment an object with irregular boundaries, Barchiesi et al. [5] proposed a variational segmentation model replacing the length term $\mathcal{H}^1(\Gamma)$ with the area of the γ-neighborhood of the edge set Γ

$$\gamma-\Gamma:=\bigcup_{x\in\Gamma}B_\gamma(x). \tag{4}$$

The aim is to capture rough boundaries of the main objects in the image u_0 while at the same time achieving the denoising effect. For a given bounded Lipschitz open set $\Omega\subset R^2$ representing the image domain, the energy proposed is

$$F_{L2}(\Gamma,c_1,c_2):=\mathcal{L}^2(\gamma-\Gamma)+\lambda\int_{\text{inside}(\Gamma)}|u_0(x,y)-c_1|^2\mathrm{d}x\mathrm{d}y+\lambda\int_{\text{outside}(\Gamma)}|u_0(x,y)-c_2|^2\mathrm{d}x\mathrm{d}y \tag{5}$$

where $\mathcal{L}^2$ is the 2-dimensional Lebesgue measure, and c_1 and c_2 are defined as with the Chan-Vese model (2)

$$c_1=\frac{\int_\Omega H(\phi)u_0\mathrm{d}x}{\int_\Omega H(\phi)\mathrm{d}x}\text{ and }c_2=\frac{\int_\Omega(1-H(\phi))u_0\mathrm{d}x}{\int_\Omega(1-H(\phi))\mathrm{d}x}. \tag{6}$$

In this way the $\mathcal{L}^2$ measure will help preserving the finely oscillating boundaries of the main objects in the image and at the same time the model will allow for infinite perimeter segmentation.

Considering $f_0 := \chi_{[0,1]}$, and a smooth version of it f, a positive decreasing function such as $f(t) = e^{-t^k}$ or $f(t) = \frac{1}{1+t^k}$ for $k \geq 1$, the $\mathcal{L}^2(\gamma - \Gamma)$ term can be rewritten as:

$$\mathcal{L}^2(\gamma - \Gamma) := \int_\Omega f_0(\frac{\text{dist}(x,\Gamma)}{\gamma})\text{d}x \approx \int_\Omega f(\frac{\text{dist}(x,\Gamma)}{\gamma})\text{d}x. \tag{7}$$

The level set approach consists of working with level set functions ϕ that are signed distance functions from their zero level set Γ, so that $f(\frac{\text{dist}(\cdot,\Gamma)}{\gamma}) = f(\frac{|\phi|}{\gamma})$. To force ϕ to look like a signed distance function, a penalization term $P(\phi)$ can be added which forces $|\nabla\phi| \leq 1$. Different ways of forcing ϕ to look like a signed distance function can be found in the literature, such as adding the term $P(\phi) = \int_\Omega (|\nabla\phi| - 1)^2 \text{d}x$ (see [18]) or $\frac{1}{p}\int_\Omega |\nabla\phi|^p \text{d}x$ (for large p) or $\Delta_\infty\phi = \frac{1}{|\nabla\phi|^2}\sum_{i,j=1}^m \phi_{x_i x_j}\phi_{x_i}\phi_{x_j}$ (suggested in Barchiesi et al. [5, 29]), or a local image fitting energy functional, which can be viewed as a constraint of the differences between the fitting image and the original image [41].

Remark It is known that if for a Γ regular curve (e.g., a smooth curve) the Minkowski content $\lim\limits_{\gamma \longrightarrow 0} \frac{\mathcal{L}^2(\gamma-\Gamma)}{2\gamma}$ exists and coincides with the usual 1-dimensional measure $\mathcal{H}^1(\Gamma)$. This means that the first term of the energy function will be an approximation of classical perimeter, and on the other hand for fixed γ the $\mathcal{L}^2(\gamma - \Gamma)$ is smaller than $2\gamma\mathcal{H}^1(\Gamma)$.

Thus by adding the signed distance function penalization term, the revised functional to be minimized is the following

$$F_{L2f}(\phi) = \int_\Omega f(\frac{|\phi|}{\gamma}) + P(\phi) + \lambda_{1L2}\int_\Omega |u_0 - c_1|^2 H(\phi)\text{d}x + \lambda_{2L2}\int_\Omega |u_0 - c_2|^2(1 - H(\phi)). \tag{8}$$

The above problem (8) can be solved by a gradient descent method by solving

$$\frac{\partial\phi}{\partial t} = \frac{k}{\gamma}\phi^{k-1}e^{-\frac{\phi}{\gamma}^k} + D_P(\phi) - \delta(\phi)\big[\lambda_{1L2}(u_0 - c_1)^2 - \lambda_{2L2}(u_0 - c_2)^2\big], \tag{9}$$

where $D_P(\phi)$ is the term derived from $P(\phi)$, $\delta(\phi)$ the approximation of the Dirac delta function, k is a large even number. Through tests, Barchiesi et al. [5] has shown that their model has the capability of removing the noise, the cornering effect, resolution and capability of keeping oscillatory parts of the boundaries by including λ_{1L2} and λ_{2L2} as well as the additional parameter γ, performs better in comparison with the Chan-Vese model [9].

2.3 The Rada-Chen model [32]

Though all commonly used and global models may be initialized to localize an object, none can be robust especially for images with nearby feature of similar intensities. To address the need of local models, an edge-based technique first proposed by Caselles at al. [6], utilizes the image gradient as an additional constraint to stop the contours on the boundaries of desired objects. Following this idea by including a priori knowledge (such as manually selecting a few starting points) of the object/feature to be segmented, semi-automatic methods have been introduced such as [3, 14, 32]. A dual level set selective segmentation model [32] has been proposed recently for the selective segmentation model, where ϕ_G and ϕ_L are respectively used to carry out global and local segmentation (the aimed selected object) of the $\Gamma_G = \partial\Omega_G$ global curve which locates all features of image u_0 and $\Gamma_L = \partial\Omega_L$ the local curve which will evolve and find the target

object's boundary. The two initial level set functions which help in the boundary extraction process $\phi_L(x,y)$ and $\phi_G(x,y)$ are Lipschitz level sets [8, 30]. Written in level set notation, the minimization energy of this model is:

$$\begin{aligned}
&F_{DLSS}(\phi_L(x,y),\phi_G(x,y),c_1,c_2)\\
&\quad=\mu_1\int_\Omega d(x,y)g(|\nabla u_0(x,y)|)|\nabla H(\phi_L(x,y))|H(\phi_G(x,y))\mathrm{d}x\mathrm{d}y+\\
&\quad\frac{\mu_{\mathrm{L}}}{2}\int_\Omega(|\nabla\phi_L(x,y)|-1)^2\mathrm{d}x\mathrm{d}y+\\
&\quad\mu_2\int_\Omega g(|\nabla u_0(x,y)|)|\nabla H(\phi_G(x,y))|\mathrm{d}x\mathrm{d}y+\\
&\quad\frac{\mu_{\mathrm{G}}}{2}\int_\Omega(|\nabla\phi_G(x,y)|-1)^2\mathrm{d}x\mathrm{d}y+\\
&\quad\lambda_{1\mathrm{G}}\int_\Omega|u_0(x,y)-c_1|^2H(\phi_G(x,y)\mathrm{d}x\mathrm{d}y+\\
&\quad\lambda_{2\mathrm{G}}\int_\Omega|u_0(x,y)-c_2|^2(1-H(\phi_G(x,y))\mathrm{d}x\mathrm{d}y+\\
&\quad\lambda_1\int_\Omega|u_0(x,y)-c_1|^2H(\phi_L(x,y)\mathrm{d}x\mathrm{d}y+\\
&\quad\lambda_2\int_\Omega|u_0(x,y)-c_1|^2(1-H(\phi_L(x,y))H(\phi_G(x,y)\mathrm{d}x\mathrm{d}y+\\
&\quad\lambda_3\int_\Omega|u_0(x,y)-c_2|^2(1-H(\phi_L(x,y))(1-H(\phi_G(x,y))\mathrm{d}x\mathrm{d}y,
\end{aligned}\tag{10}$$

where the two quantities, an edge detector $g(u_0(x,y))$ and a distance function $d(x,y)$, have the property that they approach zero when (x,y) are near Γ, and is large when away from it. The distance and the edge detector function similar to [3, 6, 14] idea, are defined as follows:

$$d(x,y)=\mathrm{dist}((x,y),\mathcal{A})=\prod_{i=1}^{n_1}\left(1-e^{-\frac{(x-x_i^*)^2}{2\tau^2}}e^{-\frac{(y-y_i^*)^2}{2\tau^2}}\right),\quad\forall(x,y)\in\Omega\tag{11}$$

where dist = distance, $\mathcal{A}$ is the given geometric markers set, τ is a positive constant and

$$g(|\nabla u_0(x,y)|)=\frac{1}{1+|\nabla G_\sigma(x,y)*u_0(x,y)|^2},\tag{12}$$

is a stoping function which controls curve evolution on arrival to the boundary. Parameters μ_1 , μ_2 , $\lambda_{1\mathrm{G}}$, $\lambda_{2\mathrm{G}},\mu_{\mathrm{L}}$, μ_{G}, λ_1, λ_2, λ_3 are all positive, $H(\phi_L(x,y))$ and $H(\phi_G(x,y))$ are the respective Heaviside functions corresponding to the local and global level set functions. Here $G_\sigma(x,y)*u_0(x,y)$ is a smooth version of $u_0(x,y)$ with Gaussian $G_\sigma(x,y)=\sigma^{-1/2}e^{-|x^2+y^2|/4\sigma}$ dealing with the cases of possible noise. The term $P(\phi)=\int_\Omega(|\nabla\phi(x,y)|-1)^2$ has been used to avoid re-initialization of both level set functions $\phi_L(x,y)$, $\phi_G(x,y)$ by automatically scaling them. Treating the non-differentiable H function by replacing it with H_ϵ a regularized Heaviside function as in [2, 8] and applying Green's identity we get two equations for the global and local

level set:

$$\begin{cases} \mu_2\delta_\epsilon(\phi_G)\nabla\cdot\left(g(x,y)\dfrac{\nabla\phi_G}{|\nabla\phi_G|}\right)+\mu_G\nabla\cdot\left((1-\dfrac{1}{|\nabla\phi_G|})\nabla\phi_G\right)+ \\ \delta_\epsilon(\phi_G)\Big(-\mu_1W(x,y)\nabla H_\epsilon(\phi_L)-\lambda_{1\mathrm{G}}(z(x,y)-c_1)^2+\lambda_{2\mathrm{G}}(z(x,y)-c_2)^2 \\ -\lambda_2(z(x,y)-c_1)^2(1-H(\phi_L))+\lambda_3(z(x,y)-c_2)^2(1-H(\phi_L)\Big)\ =0, \quad \text{in } \Omega \end{cases} \tag{13}$$

and

$$\begin{cases} \mu_1\delta_\epsilon(\phi_L)\nabla\cdot\left(dg(|\nabla u_0|H_\epsilon(\phi_G)\dfrac{\nabla\phi_L}{|\nabla\phi_L|}\right)+\mu_L\nabla\cdot\left((1-\dfrac{1}{|\nabla\phi_L|})\nabla\phi_L\right)+ \\ \delta_\epsilon(\phi_L)\Big(-\lambda_1(u_0(x,y)-c_1)^2+\lambda_2(u_0(x,y)-c_1)^2H_\epsilon(\phi_G)+ \\ \qquad \lambda_3(u_0(x,y)-c_2)^2(1-H_\epsilon(\phi_G))\Big)\ =0, \quad \text{in } \Omega \end{cases} \tag{14}$$

with $\frac{\partial\phi_G}{\partial\vec{n}}=\frac{\partial\phi_L}{\partial\vec{n}}=0$ on $\partial\Omega$, c_1 and c_2 computed as:

$$c_1=\frac{\lambda_{1\mathrm{G}}\int_\Omega zH_\epsilon(\phi_G)\mathrm{d}x\mathrm{d}y+\lambda_1\int_\Omega zH_\epsilon(\phi_L)\mathrm{d}x\mathrm{d}y+\lambda_2\int_\Omega z(1-H_\epsilon(\phi_L))H_\epsilon(\phi_G)\mathrm{d}x\mathrm{d}y}{\lambda_{1\mathrm{G}}\int_\Omega H_\epsilon(\phi_G)\mathrm{d}x\mathrm{d}y+\lambda_1\int_\Omega H_\epsilon(\phi_L)\mathrm{d}x\mathrm{d}y+\lambda_2\int_\Omega(1-H_\epsilon(\phi_L))H_\epsilon(\phi_G)\mathrm{d}x\mathrm{d}y}, \tag{15}$$

$$c_2=\frac{\lambda_{2\mathrm{G}}\int_\Omega z(1-H_\epsilon(\phi_G))\mathrm{d}x\mathrm{d}y+\lambda_3\int_\Omega z(1-H_\epsilon(\phi_L))(1-H_\epsilon(\phi_G))\mathrm{d}x\mathrm{d}y}{\lambda_{2\mathrm{G}}\int_\Omega(1-H_\epsilon(\phi_G))\mathrm{d}x\mathrm{d}y+\lambda_3\int_\Omega(1-H_\epsilon(\phi_L))(1-H_\epsilon(\phi_G))\mathrm{d}x\mathrm{d}y} \tag{16}$$

with the assumption that $\phi_G(x,y)$, $\phi_L(x,y)$ have neither empty interior nor empty exterior.

A balloon term, which controls the contours to shrink or extend, has been incorporated in order to enlarge the capture range of the force. In this way, equations (15)-(16) are written as

$$\begin{cases} \mu_2\delta_\epsilon(\phi_G)\nabla\cdot\left(g(x,y)\dfrac{\nabla\phi_G}{|\nabla\phi_G|}\right)+\mu_G\nabla\cdot\left((1-\dfrac{1}{|\nabla\phi_G|})\nabla\phi_G\right)+ \\ \delta_\epsilon(\phi_G)\Big(-\mu_1W(x,y)\,|\nabla H_\epsilon(\phi_L)|-\lambda_{1\mathrm{G}}(z(x,y)-c_1)^2+\lambda_{2\mathrm{G}}(z(x,y)-c_2)^2- \\ \lambda_2(z(x,y)-c_1)^2(1-H(\phi_L))+\lambda_3(z(x,y)-c_2)^2(1-H(\phi_L))\Big)\ +\ \alpha g(x,y)|\nabla\phi_G|=0, \quad \text{in } \Omega \end{cases} \tag{17}$$

and

$$\begin{cases} \mu_1\delta_\epsilon(\phi_L)\nabla\cdot\left(d(x,y)g(|\nabla u_0|H_\epsilon(\phi_G)\dfrac{\nabla\phi_L}{|\nabla\phi_L|}\right)+\mu_L\nabla\cdot\left((1-\dfrac{1}{|\nabla\phi_L|})\nabla\phi_L\right)+ \\ \delta_\epsilon(\phi_L)\Big(-\lambda_1(u_0(x,y)-c_1)^2+\lambda_2(u_0(x,y)-c_1)^2H_\epsilon(\phi_G)+ \\ \qquad \lambda_3(u_0(x,y)-c_2)^2(1-H_\epsilon(\phi_G))\Big)\ +\ \alpha d(x,y)g(|\nabla u_0||\nabla\phi_L|=0, \quad \text{in } \Omega \end{cases} \tag{18}$$

where $\frac{\partial\phi_G}{\partial\vec{n}}=\frac{\partial\phi_L}{\partial\vec{n}}=0$ on $\partial\Omega$.

We remark that there exist other ways of defining geometric constraints and corresponding selective models; see [28] and the references therein for details. However it remains to generalize such methods to model infinite perimeter problems.

3. A new dual level set model for infinite perimeter

To obtain satisfactory segmentation results for image features with oscillatory boundaries,

we now equip our variational model with a new length term for regularization using $\mathcal{H}^1$ with the γ-neighborhood area of the contour Γ. For this reason, replacement of the weighted length term in the equation (10) with the area of the γ-neighborhood area of the edge set Γ is the key. In our model we consider $\mathcal{L}^2(\gamma - \Gamma) \approx \int_\Omega e^{-\frac{\phi(h)^k}{\gamma^k}}$, for a large and even number k, which is an approximation of the γ-neighborhood area in a given image $u_0(x, y)$. Similar to the level set selective segmentation models [3, 14, 15, 32, 40] as dipicted in Figure 1, for defining geometrical points in a set $\mathcal{A} = \{w_i^* = (x_i^*, y_i^*) \in \Omega,\ 1 \le i \le n_1\} \subset \Omega$, consisting of n_1 distinct points near the object, we hope to detect the features that are defined in a closed domain and to be closest to $\mathcal{A}$. The quantities $d(x, y)$ and $g(x, y)$, respectively the distance and edge detection functions, and their property of approaching zero when we are near the Γ boundary and big when away from it, can be used as a stoping function for the curve evolution.

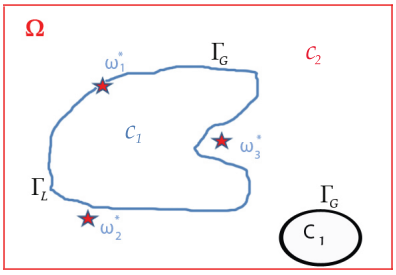

Figure 1 The numerical solution of (15) with $n = 4, m = 2$

3.1 The new model

In this work, we are particularly interested in the case of separating a feature of u_0 that has similar or identical image intensities (near some value c_1) to neighbouring features. Where an interested feature has distinctly different intensities from all neighbouring objects, past models [3, 14] are already satisfactory. As mentioned, we also assume that our image u_0 has features with irregular and oscillatory boundaries.

Using the Lipschitz level set function the energy function of our new model can be written:

$$\begin{aligned}
&\min_{\phi_L(x,y),\phi_G(x,y),c_1,c_2} F_{IDLSS}(\phi_L, \phi_G, c_1, c_2) \\
&= \mu_1 \int_\Omega d(x,y) g(\nabla u_0) e^{-(\frac{\phi_L}{\gamma})^k} H(\phi_G) + \frac{\mu_{\mathrm{L}}}{2} \int_\Omega (|\nabla \phi_L| - 1)^2 \mathrm{d}x\mathrm{d}y + \\
&\quad \mu_2 \int_\Omega g(\nabla u_0) e^{-(\frac{\phi_G}{\gamma})^k} + \frac{\mu_{\mathrm{G}}}{2} \int_\Omega (|\nabla \phi_G(x,y)| - 1)^2 \mathrm{d}x\mathrm{d}y + \\
&\quad \lambda_{1\mathrm{G}} \int_\Omega |u_0(x,y) - c_1|^2 H(\phi_G(x,y) \mathrm{d}x\mathrm{d}y + \\
&\quad \lambda_{2\mathrm{G}} \int_\Omega |u_0(x,y) - c_2|^2 (1 - H(\phi_G(x,y)) \mathrm{d}x\mathrm{d}y + \\
&\quad \lambda_1 \int_\Omega |u_0(x,y) - c_1|^2 H(\phi_L(x,y) \mathrm{d}x\mathrm{d}y +
\end{aligned}$$

$$\lambda_2 \int_\Omega |u_0(x,y) - c_1|^2 (1-H)(\phi_L(x,y)) H(\phi_G(x,y) \mathrm{d}x\mathrm{d}y +$$
$$\lambda_3 \int_\Omega |u_0(x,y) - c_2|^2 (1-H)(\phi_L(x,y))(1-H(\phi_G(x,y)) \mathrm{d}x\mathrm{d}y \tag{19}$$

where ϕ_L, ϕ_G, c_1, c_2, μ_1, μ_2, $\lambda_{1\mathrm{G}}$, $\lambda_{2\mathrm{G}}$, μ_{L}, μ_{G}, λ_1, λ_2, λ_3, $H(\phi_L)$, $H(\phi_G)$ are defined as for (10). Here the terms $\lambda_1, \lambda_{1G}, \lambda_2$ allow the total freedom of the level set functions so that ϕ_L will not pick up spurious features nearby.

Different regularized Heaviside functions can be used e.g.

$$H_\epsilon^I = \begin{cases} 0, & z < -\epsilon \\ \frac{1}{2}\left[1 + \frac{z}{\epsilon} + \frac{1}{\pi}\sin(\frac{\pi z}{\epsilon})\right], & |z| \leq \epsilon, \\ 1, & z > \epsilon, \end{cases}$$

$$H_\epsilon^{II} = \frac{1}{2}(1 + \mathrm{erf}(\frac{\epsilon}{z})), \quad H_\epsilon^{III} = \frac{1}{2}(1 + \frac{2}{\pi}\arctan(\frac{z}{\epsilon})),$$

where $\mathrm{erf}(x)$ is twice the integral of the Gaussian distribution with 0 mean and variance of $\frac{1}{2}$ in the form $\mathrm{erf}(x) = \frac{2}{\sqrt{\pi}}\int_0^x e^{-t^2}\mathrm{d}t$. H_ϵ^I and H_ϵ^{II} and their corresponding delta function δ_ϵ^I and δ_ϵ^{II} have a smaller support in the interval $[-\epsilon, \epsilon]$, while H_ϵ^{III} and its corresponding δ_ϵ^{III} are different from zero everywhere. This observation suggests that H_ϵ^{III} may be suitable for global feature extraction, while H_ϵ^I, or H_ϵ^{II} are to be used for the selective segmentation. In this way the model can be written:

$$\begin{aligned}
&\min_{\phi_L(x,y),\phi_G(x,y),c_1,c_2} F_{IDLSS}(\phi_L, \phi_G, c_1, c_2) \\
&= \mu_1 \int_\Omega d(x,y) g(\nabla u_0) e^{-(\frac{\phi_L}{\gamma})^k} H_\epsilon(\phi_G) + \frac{\mu_{\mathrm{L}}}{2}\int_\Omega (|\nabla\phi_L| - 1)^2 \mathrm{d}x\mathrm{d}y + \\
&\quad \mu_2 \int_\Omega g(\nabla u_0) e^{-(\frac{\phi_G}{\gamma})^k} + \frac{\mu_{\mathrm{G}}}{2}\int_\Omega (|\nabla\phi_G(x,y)| - 1)^2 \mathrm{d}x\mathrm{d}y + \\
&\quad \lambda_{1\mathrm{G}} \int_\Omega |u_0(x,y) - c_1|^2 H_\epsilon(\phi_G(x,y) \mathrm{d}x\mathrm{d}y + \\
&\quad \lambda_{2\mathrm{G}} \int_\Omega |u_0(x,y) - c_2|^2 (1 - H_\epsilon(\phi_G(x,y)) \mathrm{d}x\mathrm{d}y + \\
&\quad \lambda_1 \int_\Omega |u_0(x,y) - c_1|^2 H_\epsilon(\phi_L(x,y) \mathrm{d}x\mathrm{d}y + \\
&\quad \lambda_2 \int_\Omega |u_0(x,y) - c_1|^2 (1 - H_\epsilon(\phi_L(x,y)) H(\phi_G(x,y) \mathrm{d}x\mathrm{d}y + \\
&\quad \lambda_3 \int_\Omega |u_0(x,y) - c_2|^2 (1 - H_\epsilon(\phi_L(x,y))(1 - H_\epsilon(\phi_G(x,y)) \mathrm{d}x\mathrm{d}y.
\end{aligned} \tag{20}$$

By keeping ϕ_L and ϕ_G fixed and deriving with respect to c_1 and c_2, we get equations for computing c_1 and c_2:

$$c_1 = \frac{\lambda_{1\mathrm{G}} \int_\Omega u_0 H_\epsilon(\phi_G)\mathrm{d}x\mathrm{d}y + \lambda_1 \int_\Omega u_0 H_\epsilon(\phi_L)\mathrm{d}x\mathrm{d}y + \lambda_2 \int_\Omega u_0(1 - H_\epsilon(\phi_L)) H_\epsilon(\phi_G)\mathrm{d}x\mathrm{d}y}{\lambda_{1\mathrm{G}} \int_\Omega H_\epsilon(\phi_G)\mathrm{d}x\mathrm{d}y + \lambda_1 \int_\Omega H_\epsilon(\phi_L)\mathrm{d}x\mathrm{d}y + \lambda_2 \int_\Omega (1 - H_\epsilon(\phi_L)) H_\epsilon(\phi_G)\mathrm{d}x\mathrm{d}y}, \tag{21}$$

$$c_2 = \frac{\lambda_{2\mathrm{G}} \int_\Omega u_0(1 - H_\epsilon(\phi_G))\mathrm{d}x\mathrm{d}y + \lambda_3 \int_\Omega u_0(1 - H_\epsilon(\phi_L))(1 - H_\epsilon(\phi_G))\mathrm{d}x\mathrm{d}y}{\lambda_{2\mathrm{G}} \int_\Omega (1 - H_\epsilon(\phi_G))\mathrm{d}x\mathrm{d}y + \lambda_3 \int_\Omega (1 - H_\epsilon(\phi_L))(1 - H_\epsilon(\phi_G))\mathrm{d}x\mathrm{d}y}, \tag{22}$$

and by keeping c_1 and c_2 fixed we get the equations for ϕ_G and ϕ_L

$$\begin{cases} \mu_2 g(\nabla u_0)\dfrac{k}{\gamma^k}\phi_G^{k-1}e^{-(\frac{\phi_G}{\gamma})^k} + \mu_G\nabla\cdot\left((1-\dfrac{1}{|\nabla\phi_G|})\nabla\phi_G\right)+ \\ \delta_\epsilon(\phi_G)\Big(-\mu_1 d(x,y)g(\nabla u_0)e^{-(\frac{\phi_L}{\gamma})^k} - \lambda_{1\mathrm{G}}(u_0(x,y)-c_1)^2 + \lambda_{2\mathrm{G}}(u_0(x,y)-c_2)^2 - \\ \lambda_2(u_0(x,y)-c_1)^2(1-H(\phi_L)) + \lambda_3(u_0(x,y)-c_2)^2(1-H(\phi_L))\Big) + \alpha g(x,y)|\nabla\phi_G| = 0, \quad \text{in } \Omega \end{cases} \tag{23}$$

and

$$\begin{cases} \mu_1 d(x,y)g(\nabla u_0)\dfrac{k}{\gamma^k}\phi_L^{k-1}e^{-(\frac{\phi_L}{\gamma})^k}H_\epsilon(\phi_G) + \mu_L\nabla\cdot\left((1-\dfrac{1}{|\nabla\phi_L|})\nabla\phi_L\right)+ \\ \delta_\epsilon(\phi_L)\Big(-\lambda_1(u_0(x,y)-c_1)^2 + \lambda_2(u_0(x,y)-c_1)^2H_\epsilon(\phi_G)+ \\ \qquad \lambda_3(zu_0(x,y)-c_2)^2(1-H_\epsilon(\phi_G))\Big) + \alpha d(x,y)g(\nabla u_0)|\nabla\phi_L| = 0, \quad \text{in } \Omega \end{cases} \tag{24}$$

with $\frac{\partial\phi_G}{\partial\vec{n}} = \frac{\partial\phi_L}{\partial\vec{n}} = 0$ on $\partial\Omega$. The terms $\alpha d(x,y)g(\nabla u_0)|\nabla\phi_L|$ and $\alpha g(x,y)|\nabla\phi_G|$ are the balloon term force. The approximation can be done by introducing an artificial time step t and getting the gradient descent method. Thus for c_1 and c_2, which will be updated at each step according to the above formula and solving

$$\begin{cases} \dfrac{\partial\phi_G}{\partial t} = \mu_2 g(\nabla u_0)\dfrac{k}{\gamma^k}\phi_G^{k-1}e^{-(\frac{\phi_G}{\gamma})^k} + \mu_G\nabla\cdot\left((1-\dfrac{1}{|\nabla\phi_G|})\nabla\phi_G\right)+ \\ \delta_\epsilon(\phi_G)\Big(-\mu_1 d(x,y)g(\nabla u_0)e^{-(\frac{\phi_L}{\gamma})^k} - \lambda_{1\mathrm{G}}(u_0(x,y)-c_1)^2 + \lambda_{2\mathrm{G}}(u_0(x,y)-c_2)^2 - \\ \lambda_2(u_0(x,y)-c_1)^2(1-H(\phi_L)) + \lambda_3(u_0(x,y)-c_2)^2(1-H(\phi_L))\Big) + \alpha g(x,y)|\nabla\phi_G| = 0 \end{cases} \tag{25}$$

and

$$\begin{cases} \dfrac{\partial\phi_L}{\partial t} = \mu_1 d(x,y)g(\nabla u_0)\dfrac{k}{\gamma^k}\phi_L^{k-1}e^{-(\frac{\phi_L}{\gamma})^k}H_\epsilon(\phi_G) + \mu_L\nabla\cdot\left((1-\dfrac{1}{|\nabla\phi_L|})\nabla\phi_L\right)+ \\ \delta_\epsilon(\phi_L)\Big(-\lambda_1(u_0(x,y)-c_1)^2 + \lambda_2(u_0(x,y)-c_1)^2H_\epsilon(\phi_G)+ \\ \qquad \lambda_3(zu_0(x,y)-c_2)^2(1-H_\epsilon(\phi_G))\Big) + \alpha d(x,y)g(\nabla u_0)|\nabla\phi_L| = 0. \end{cases} \tag{26}$$

After solving these equations, the local level set $\phi_L \leq 0$ will define the selected object.

3.2 An additive operator splitting algorithm

To develop a fast and a low computational cost method for solving equations (25) and (26), we can use the idea of the additive operator splitting (AOS) method (similar to the classical operator splitting methods), proposed by Tai et al. [21] and Weickert [39] and widely applied to a diffusion equation, such as [3, 15, 38]. The main idea of the method is to transfer a semi-implicit linear system into an additive solvable linear system. To implement this method in our algorithm we first make the discretization of the diffusion equation, form a semi-implicit linear system and develop the iterative approximation scheme which solves a diagonally dominant tridiagonal linear system.

In order to develop an additive operator splitting (AOS) method for (25) and (26), we consider the following related parabolic equations with $\frac{\partial \phi_L}{\partial \vec{n}}\big|_{\partial\Omega} = \frac{\partial \phi_G}{\partial \vec{n}}\big|_{\partial\Omega} = 0$:

$$\begin{cases} \dfrac{\partial \phi_L}{\partial t} = \mu_{\mathrm{L}} \nabla \cdot (E_L \nabla \phi_L) + f_L \ = \mu_{\mathrm{L}}(\partial_x(E_L \partial_x \phi_L) + \partial_y(E_L \partial_y \phi_L)) + f_L, \\ \dfrac{\partial \phi_G}{\partial t} = \mu_{\mathrm{G}} \nabla \cdot (E_G \nabla \phi_G) + f_G \ = \mu_{\mathrm{G}}(\partial_x(E_G \partial_x \phi_G) + \partial_y(E_G \partial_y \phi_G)) + f_G, \end{cases} \tag{27}$$

where

$$\begin{aligned} f_L =& d(x,y) g(\nabla u_0) \frac{k}{\gamma^k} \phi_L^{k-1} e^{-(\frac{\phi_L}{\gamma})^k} H_\epsilon(\phi_G) + \delta_\epsilon(\phi_L) \Big(-\lambda_1 (u_0(x,y) - c_1)^2 + \\ & \lambda_2 (u_0(x,y) - c_1)^2 H_\epsilon(\phi_G) \ + \lambda_3 (u_0(x,y) - c_2)^2 (1 - H_\epsilon(\phi_G)) \Big) + d(x,y) g(\nabla u_0) |\nabla \phi_L|, \\ f_G =& \mu g(\nabla u_0) \frac{k}{\gamma^k} \phi_G^{k-1} e^{-(\frac{\phi_G}{\gamma})^k} + \delta_\epsilon(\phi_G) \Big(-\mu_1 d(x,y) g(\nabla u_0) e^{-(\frac{\phi_L}{\gamma})^k} - \lambda_{1\mathrm{G}} (u_0(x,y) - c_1)^2 + \\ & \lambda_{2\mathrm{G}} (u_0(x,y) - c_2)^2 - \lambda_2 (u_0(x,y) - c_1)^2 (1 - H(\phi_L)) + \lambda_3 (u_0(x,y) - c_2)^2 (1 - H(\phi_L)) \Big) + \\ & \alpha g(x,y) |\nabla \phi_G|, \\ W =& d(x,y) g(\nabla u_0), \quad E_L = 1 - \frac{1}{|\nabla \phi_L|}, \quad E_G = 1 - \frac{1}{|\nabla \phi_G|}. \end{aligned}$$

It suffices to consider how to solve a general equation:

$$\frac{\partial \phi}{\partial t} = \mu(\partial_x(E \partial_x \phi) + \partial_y(E \partial_y \phi)) + f. \tag{28}$$

The equation can be rewritten in the matrix-vector form:

$$\frac{\phi^{n+1} - \phi^n}{\Delta t} = \sum_{l=1}^{m} A_l(\phi^n) \phi^{n+1} + f(x,y),$$

where Δt is the time step size, m is 2 since we are dealing with two dimensions, n denotes the n^{th} iteration and A_l is diffusion quantity in l direction ($l = 1$ and $l = 2$, respectively, for x and y direction for the two dimensional case). We can rewrite the above equation in the semi-implicit form:

$$\phi^{n+1} = (\ I - \Delta t \sum_{l=1}^{m} A_l(\phi^n))^{-1}\ \hat{\phi}^n \text{ for } l = 1,2 \text{ and } \hat{\phi}^n = \phi^n + \Delta t f(x,y)$$

which by employing the AOS scheme can be split additively as shown below to define the AOS solution

$$\phi^{n+1} = \frac{1}{m} \sum_{l=1}^{m} (I - m \Delta t A_l(\phi^n))^{-1}\ \hat{\phi}^n. \tag{29}$$

Here for equation (28), A_l for $l = 1, 2$ are tridiagonal matrices derived using finite differences:

$$\begin{aligned} (A_1(\phi^n)\phi^{n+1})_{i,j} &= \mu \Big(\partial_x (E \partial_x \phi^{n+1}) \Big)_{i,j} \\ &= \mu \frac{E^n_{i+1/2,j} (\partial_x \phi^{n+1})_{i+1/2,j} - E^n_{i-1/2,j} (\partial_x \phi^{n+1})_{i-1/2,j}}{h_x} \\ &= \mu \frac{\frac{E^n_{i+1,j} + E^n_{i,j}}{2} (\frac{\phi^{n+1}_{i+1,j} - \phi^{n+1}_{i,j}}{h_x}) - \frac{E^n_{i,j} + E^n_{i-1,j}}{2} (\frac{\phi^{n+1}_{i,j} - \phi^{n+1}_{i-1,j}}{h_x})}{h_x} \end{aligned}$$

$$
\begin{aligned}
&= \mu \frac{E^n_{i+1,j} + E^n_{i,j}}{2h_x^2}(\phi^{n+1}_{i+1,j} - \phi^{n+1}_{i,j}) - \frac{E^n_{i,j} + E^n_{i-1,j}}{2h_x^2}(\phi^{n+1}_{i,j} - \phi^{n+1}_{i-1,j}),\\
(A_2(\phi^n)\phi^{n+1})_{i,j} &= \mu \left(\partial_y (E \partial_y \phi^{n+1}) \right)_{i,j}\\
&= \mu \frac{E^n_{i,j+1/2}(\partial_y \phi^{n+1})_{i,j+1/2} - E^n_{i,j-1/2}(\partial_y \phi^{n+1})_{i,j-1/2}}{h_y}\\
&= \mu \frac{\frac{E^n_{i,j+1}+E^n_{i,j}}{2}\left(\frac{\phi^{n+1}_{i,j+1}-\phi^{n+1}_{i,j}}{h_x}\right) - \frac{E^n_{i,j}+E^n_{i,j-1}}{2}\left(\frac{\phi^{n+1}_{i,j}-\phi^{n+1}_{i,j-1}}{h_y}\right)}{h_y}\\
&= \mu \frac{E^n_{i,j+1} + E^n_{i,j}}{2h_y^2}(\phi^{n+1}_{i,j+1} - \phi^{n+1}_{i,j}) - \frac{E^n_{i,j} + E^n_{i,j-1}}{2h_y^2}(\phi^{n+1}_{i,j} - \phi^{n+1}_{i,j-1}).
\end{aligned}
$$

The following iteration procedure has been designed for the model:

Step 1. Define the markers and associated parameters based on the image being considered;

Step 2. Calculate the edge based and distance function;

Step 3. Design the initial level sets ϕ_L and ϕ_G;

Step 4. Compute ϕ_L and ϕ_G according to (29);

Step 5. Check convergence $\frac{\|\phi_L^{n+1} - \phi_L^n\|}{\|\phi_L^n\|} < \varepsilon$. If satisfied, stop. Otherwise, go back to Step 3.

4. Experimental results

To verify the performance of our new method, experiments were carried out on images with oscillating boundaries. First we present experimental results demonstrating our segmentation method results for segmenting a selective object. Next, we present the comparison of the new model with the DLSS model in some experimental results. Lastly, we present experimental results of a more challenging problem, where the object shapes have oscillatory boundaries.

Our method is based on the same user defined information, such as the markers, and some parameters which need to be adjusted according to the given image, such as a smoothing factor and the balloon force coefficient. In our numerical experiments, for the AOS algorithm, $h = 1$ (the step space), $\triangle t = 1$ (the time step), $\alpha = -0.01$, $\tau = 4$, $\mu_{\mathrm{L}} = \mu_{\mathrm{G}} = 10^{-3}$. Different image sizes have been tested $n = 128, 180, 256, 512$. Different values for $\lambda_s = \lambda_{1G} = \lambda_{2G} = \lambda_1 = \lambda_2 = \lambda_3$ have been chosen and show that the method performs well and gets similar results. For the following experiment we will show results of choice for μ_s and λ_s such that:

$\lambda_s = \lambda_{1G} = \lambda_{2G} = \lambda_1 = \lambda_2 = \lambda_3 = 300$, $\mu_s = \mu_1 = \mu_2 = 1$ or

$\lambda_s = \lambda_{1G} = \lambda_{2G} = \lambda_1 = \lambda_2 = \lambda_3 = 300$, $\mu_s = \mu_1 = \mu_2 = 200$ or

$\lambda_s = \lambda_{1G} = \lambda_{2G} = \lambda_1 = \lambda_2 = \lambda_3 = 80$, $\mu_s = \mu_1 = \mu_2 = 1$ or

$\lambda_s = \lambda_{1G} = \lambda_{2G} = \lambda_1 = \lambda_2 = \lambda_3 = 300$, $\mu_s = \mu_1 = \mu_2 = n^2/10$.

Other different μ_s and λ_s have also been chosen and we found that the results are similar. The initial global level set, placed as a circle, has the form

$$\phi_G^0 = \sqrt{(x - x_G^0)^2 + (y - y_G^0)^2} - r_G^0$$

(where (x_G^0, y_G^0) is the center of the circle), and the initial local level set is placed similarly to the time marching algorithm, previously mentioned in Section 3. Since $H_{3\epsilon}$ has a bigger support in

the interval $[-\epsilon, \epsilon]$, which means that with it a moderately large ϵ may lead to spurious results, in our experiments for the local level set, as approximations for the heaviside function we use $H_{1\epsilon}$ or $H_{2\epsilon}$ with $\epsilon = h = 1$, and for the global level set $H_{3\epsilon}$ with $\epsilon = h = 1$.

4.1 Test Set 1–robustness of the new model

In this section, we demonstrate the ability of recognizing specific objects by our infinite perimeter segmentation algorithm on some synthetic and real life images.

First, in Test Set 1, Figures 2 and 3 present experimental results using the time marching algorithm for the new dual level set model. The algorithm is based on contracting or expanding the initial curve, therefore the initial curve has to be nearby (inside or outside) the given object. As prior information is given (markers) they can be used in the construction of the local level set. The initial local contour can be a circle such that the center and the radius are $\mathbf{w_0} = (x_0, y_0) = (\frac{1}{n_1}\sum_{i=1}^{n_1} x_i^*, \frac{1}{n_1}\sum_{i=1}^{n_1} y_i^*)$ and $r = \min_i |\mathbf{w}_i^* - \mathbf{w}_0|$, respectively, where $\mathbf{w}_i^* = (x_i^*, y_i^*)$. In cases the objects are near (which happens often in such processes), the shape is irregular or we want to start with a better nearby level-set, a distant function level-set constructed with the polygon of the given markers can be used. This initialization has been found as more proper in our experiments. Figure 3 shows the local and global level-set initialization. The images chosen for the experiments have different sizes such as $n = 128$ (i.e., 128×128), $n = 180$ (i.e., 180×180), and $n = 256$ (i.e., 256×256), and the parameters tested are $k = 8$, $\gamma = 10$, $\lambda_1 = \lambda_2 = \lambda_3 = \lambda_{1G} = \lambda_{2G} = 100$, $\tau = 4$, $h = 1$, $\mu_1 = \mu_2 = 1$, $\mu_L = \mu_G = 0.0001$, $\gamma = 5$, $\epsilon = 1$ and $\Delta t = 0.01$. Other parameters for $\lambda_s = \lambda_1 = \lambda_2 = \lambda_3 = \lambda_{1G} = \lambda_{2G}$, and $\mu_s = \mu_1 = \mu_2$ can be chosen and it can be shown that the results of the method are similar. To speed up convergence, the AOS algorithm has been used as a faster solver compared with time marching. In this case comparing with explicit time marching, Δt (the time step) is not required to be particularly small.

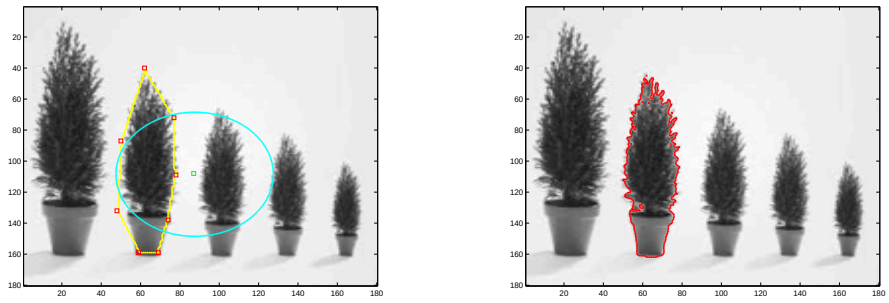

(a) Initial local (yellow) and global (cyan) level sets ($n = 180$);

(b) Real life image successfully selected ($n = 180$)

Figure 2 Successful segmentation with the time marching algorithm for infinite selective segmentation model of the vase with markers set in the boundary of second vase (aimed object).

Next, we are showing here the numerical results of our new method for segmenting 7 different images applying time marching or the AOS method. In Figure 2(b), we show that the model works satisfactorily with the time marching algorithm for a real life image. Similar to Figure 2, Figure 3 has been processed with the time marching algorithm in four different test results, from

which the first two images show that the model works satisfactorily for cases where the features are nearby, meanwhile Figures 3(c) and (d) show the successful segmentation of biological and medical images. The images of Figure 3 give similar results when processed with the AOS method, and for the sake of brevity we do not show them again. Images in Figure 4 show the results obtained using the AOS method. Figure 4(b) shows results obtained from segmentation of images with strong additive noise of the trees image. Figures 4 (c) and (d) show the segmentation of a leaf collection picture with different shapes and close to each other. All of these figures show that by giving some points in the object the model does not get attracted to the other object with the same intensity.

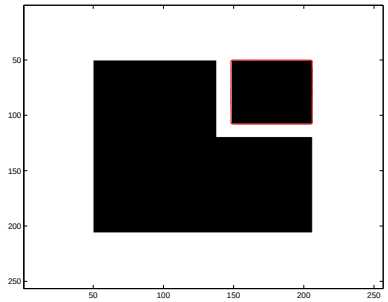

(a) Geometric image with the markers set in the corner of the rectangle ($n = 256$)

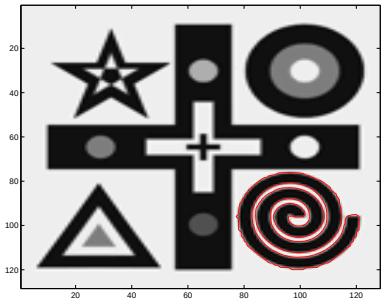

(b) Successful segmentation of the spirals with the time marching ($n = 126$)

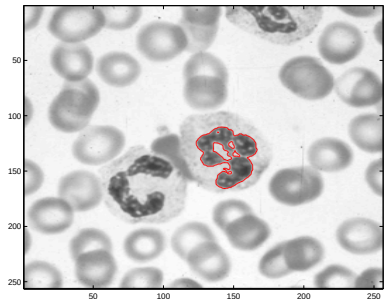

(c) Cells embryo successfully selected ($n = 256$)

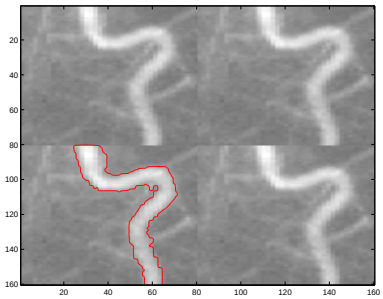

(d) Successful selective segmentation of blood vessel in an repeated image ($n = 180$)

Figure 3 Successful segmentation with the new algorithm for infinite selective segmentation model

4.2 Test Set 2–comparison with the previous Rada-Chen model [32]

We now compare our model with the DLSS method [32] for 4 easier problems, as shown in Figures 5–8. In the case of Figures 5 and 6, we can see that for the testing examples, both models give almost the same result. For the test results in Figures 7 and 8 both models give almost the same result except for the fact that the new model is showing the empty place between the leafs much more accurately.

4.3 Test Set 3–improvement of the new model over Rada-Chen [32]

Test problems 3 are more challenging due to the oscillatory boundaries of the objects. In particular, we consider the problem of segmenting brush-like pine trees which clearly have

oscillatory boundaries; here the cornering effect of the model can be observed. The results of our new segmentation method are shown in Figures 9, 11, 13, 15, 17 and 19, which appear to be quite accurate despite the low-quality data. In these cases, the previous models from [32] will lose some details. Figures 9, 11, 13, 15, 17 and 19 and the respective cropping Figures 10, 12, 14, 16, 18 and 20, show better results when oscillatory boundaries are present. In each case, the left row image shows the results of [32] and the right image shows the correctly segmented results by our new model.

5. Conclusions

In this paper we presented a new variational model with two level set functions (one for global segmentation and the other for local and selective segmentation) for reliable and localized segmentation, improving on previous work. A Lebesgue measure which leads to no limitation of the perimeter segmentation has been incorporated. The selective segmentation is based on optimization of a distance function, an edge detection function, and the region information. We derived the curve evolution equations for the problem posed in the variational framework and demonstrated the effectiveness of the resulting algorithm in segmenting a variety of images. Numerical experiments show that the new model delivers similar results for general problems to old models and improved results for the problems where the boundary has oscillation.

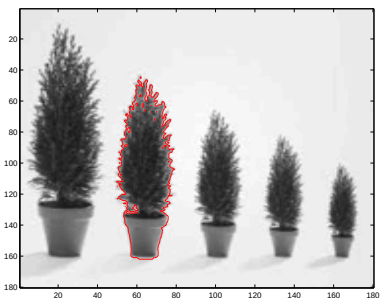

(a) Real life image ($n = 180$)

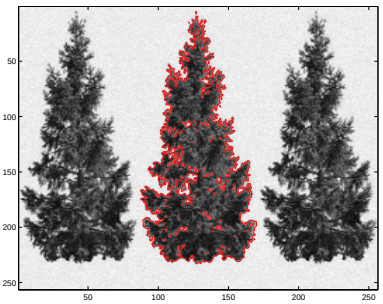

(b) Real life image with 10% additive noise ($n = 180$)

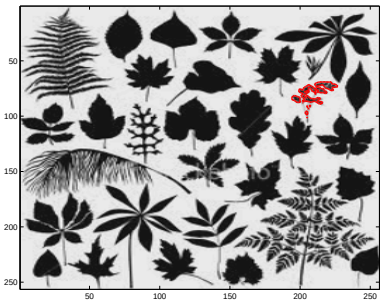

(c) Real life image ($n = 250$)

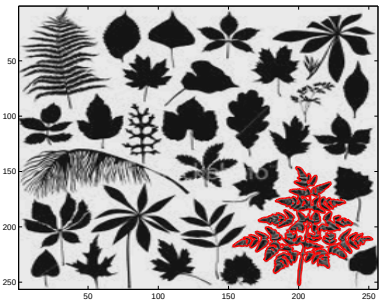

(d) Real life image ($n = 250$)

Figure 4 Successful segmentation with the AOS infinite selective segmentation model, with $dt = 1$, $\mu_s = 1$, $\lambda_s = 300$

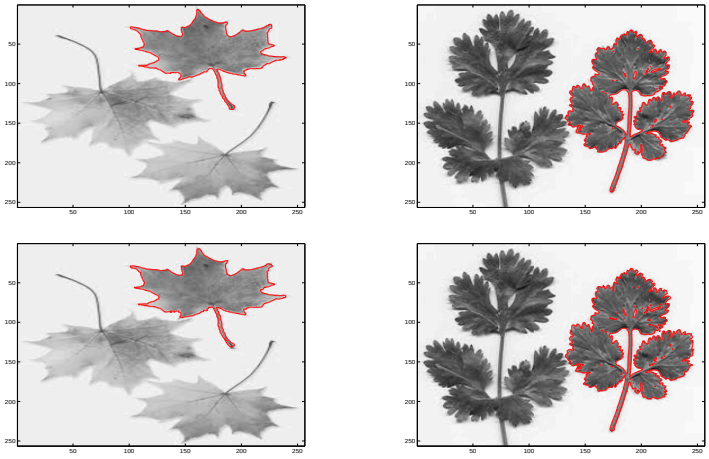

Figure 5 First row old model with H^1 Hausdorff measurement, $dt = 1$, $\mu_s = 1$, $\lambda_s = 80$; second row new model with L^2 measurement, $dt = 1$, $\mu_s = 1$ $\lambda_s = 80$

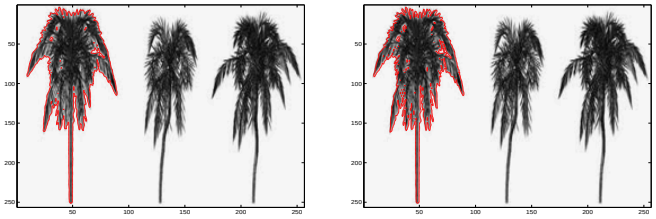

Figure 6 First picture: old model with H^1 Hausdorff measurement, $dt = 1$, $\mu_s = mn/10$ $\lambda_s = 300$; second picture: new model with L^2 measurement

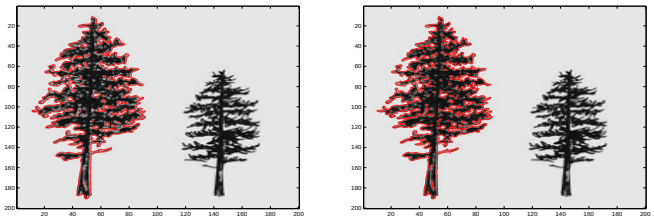

Figure 7 First picture: old model with H^1 Hausdorff measurement, $dt = 1$, $\mu_s = mn/10$ $\lambda_s = 300$; second picture: new model with L^2 measurement

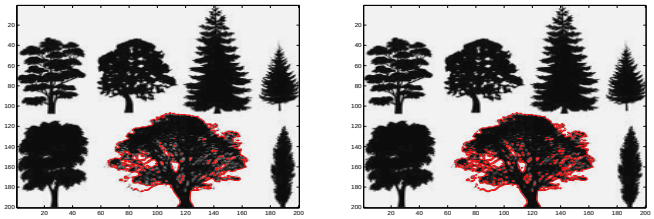

Figure 8 First picture: old model with H^1 Hausdorff measurement, $dt = 1$, $\mu_s = mn/10$ $\lambda_s = 300$; second picture: new model with L^2 measurement

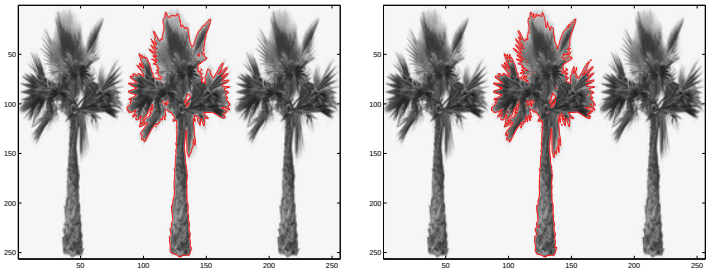

Figure 9 First picture: old model with H^1 Hausdorff measurement, $dt = 1$, $\mu_s = 1$ $\lambda_s = 300$; second picture: new model with L^2 measurement

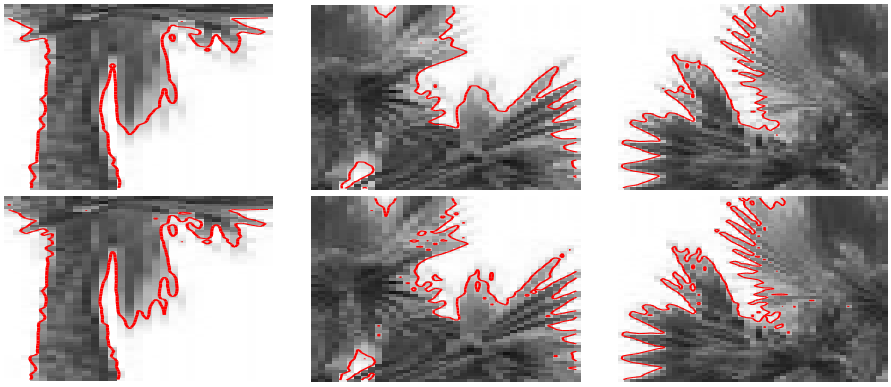

Figure 10 First picture: old model with H^1 Hausdorff measurement, $dt = 1$, $\mu_s = 200$ $\lambda_s = 300$; second picture: new model with L^2 measurement (cropping)

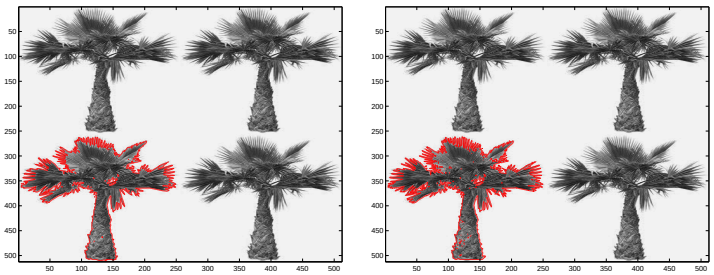

Figure 11 First picture: old model with H^1 Hausdorff measurement, $dt = 1$, $\mu_s = 1$ $\lambda_s = 300$; second picture: new model with L^2 measurement

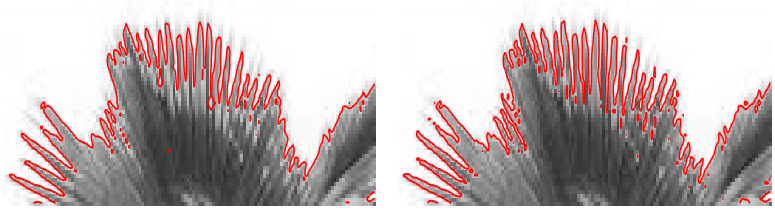

Figure 12 First picture: old model with H^1 Hausdorff measurement, $dt = 1$, $\mu = mn/10$ $\lambda = 300$; second picture: new model with L^2 measurement (cropping)

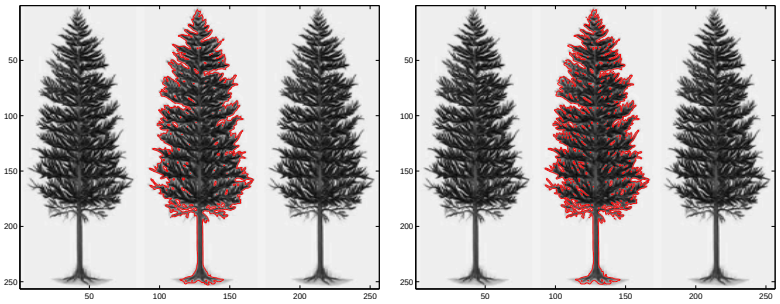

Figure 13 First picture: old model with H^1 Hausdorff measurement, $dt = 1$, $\mu_s = 1$ $\lambda_s = 300$; second picture: new model with L^2 measurement

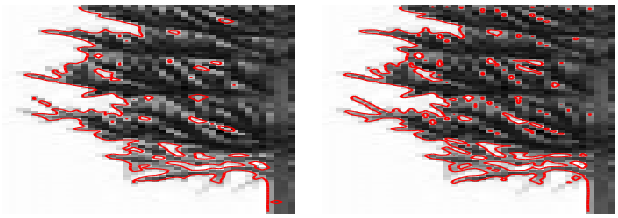

Figure 14 First picture: old model with H^1 Hausdorff measurement, $dt = 1$, $\mu_s = mn/10$ $\lambda = 300$; second picture: new model with L^2 measurement (cropping)

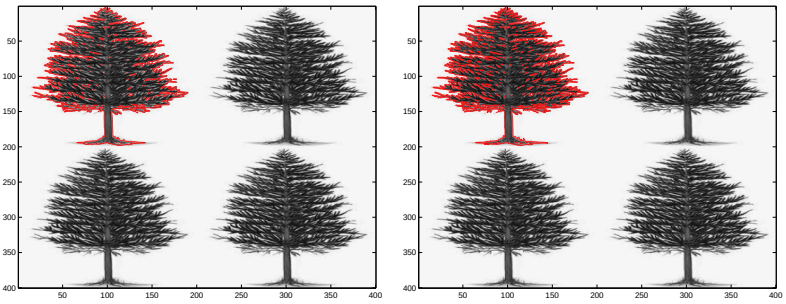

Figure 15 First picture: old model with H^1 Hausdorff measurement, $dt = 1$, $\mu_s = 1$ $\lambda_s = 300$; second picture: new model with L^2 measurement

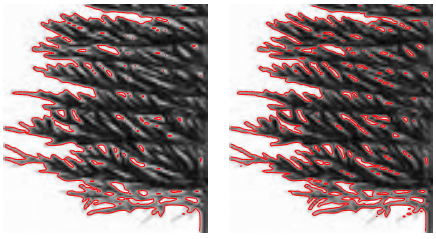

Figure 16 First picture: old model with H^1 Hausdorff measurement, $dt = 1$, $\mu_s = mn/10$ $\lambda_s = 300$; second picture: new model with L^2 measurement (cropping)

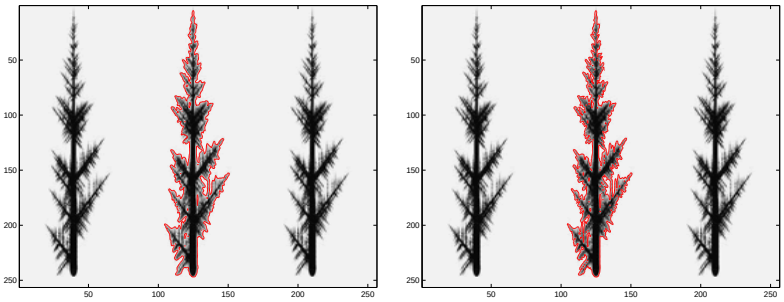

Figure 17 First picture: old model with H^1 Hausdorff measurement, $dt = 1$, $\mu_s = nm/10$ $\lambda_s = 300$; second picture: new model with L^2 measurement

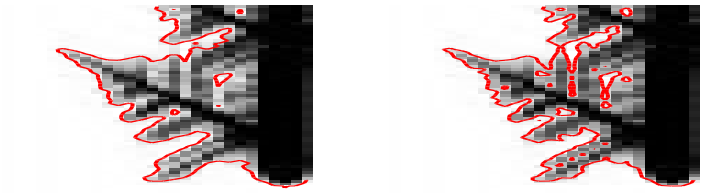

Figure 18 First picture: old model with H^1 Hausdorff measurement, $dt = 1$, $\mu_s = mn/10$ $\lambda_s = 300$; second picture: new model with L^2 measurement (cropping)

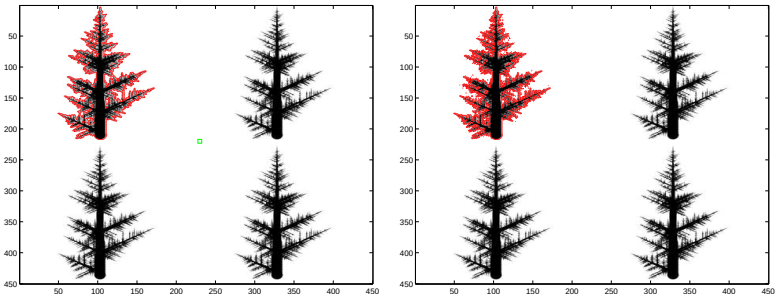

Figure 19 First picture: old model with H^1 Hausdorff measurement, $dt = 1$, $\mu_s = mn/10$ $\lambda_s = 300$; second picture: new model with L^2 measurement

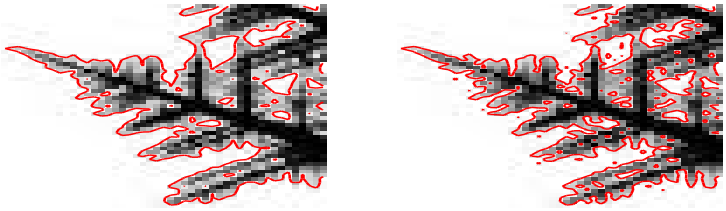

Figure 20 First picture: old model with H^1 Hausdorff measurement, $dt = 1$, $\mu_s = mn/10$ $\lambda_s = 300$; second picture: new model with L^2 measurement cropping

References

[1] R. ADAMS, L. BISCHOF. *Seeded region growing*. IEEE Transactions on Pattern Analysis and Machine Intelligence, 1994, **16**(6): 641–647.

[2] G. AUBERT, P. KORNPROBST. *Mathematical Problems in Image Processing: Partial Differential Equations and the Calculus of Variations*. Springer, 2001.

[3] Noor BADSHAH, Ke CHEN. *Image selective segmentation under geometrical constraints using an acftive contour approach*. Commun. Comput. Phys., 2009, **7**(4): 759–778.

[4] E. BAE, X. C. TAI. *Graph cuts for the multiphase Mumford-Shah model using piecewise constant level set methods*. In K. Jun, C. Keem, H. Lee and J. Choi, editors, Proceedings of the National Institute for Mathematical Sciences, 127–135, NIMS, Korea, 2008.

[5] Marco BARCHIESI, Sung H. KANG, Triet LE, et al. *A variational model for infinite perimeter segmentations based on Lipschitz level set functions: denoising while keeping finely oscillatory boundaries*. Multiscale Model. Simul., 2010, **8**(5): 1715–1741.

[6] V. CASELLES, R. KIMMEL, G. SAPIRO. *Geodesic active contours*. International Journal of Computer Vision, 1997, **22**(1): 61–79.

[7] Tony F. CHAN, J. H. SHEN. *Image Processing and Analysis-Variational, PDE, Wavelet, and Stochastic Methods*. SIAM Publications, Philadelphia, USA, 2005.

[8] Tony F. CHAN, L. A. VESE. *An active contour model without edges*. In Lecture Notes in Computer Science, Volume 1682, 141–151, 1999.

[9] Tony F. CHAN, L. A. VESE. *Active contours without edges*. IEEE Transactions on Image Processing, 2001, **10**(2): 266–277.

[10] Ginmo CHUNG, L. A. VESE. *Image segmentation using a multilayer level-set approach*. Computing and Visualization in Science, 2009, **12**: 267–285.

[11] L. COHEN. *On active contour models and balloons*. Comp. Vision, Graphics and Image Proc: Image Understanding, 1991, **53**(2): 211–218.

[12] Dorin COMANICIU, Peter MEER. *Mean shift: A robust approach toward feature space analysis*. IEEE Transactions on Pattern Analysis and Machine Intelligence, 2002, **24**(5): 603–619.

[13] Stuart GEMAN, Donald GEMAN. *Stochastic relaxation, Gibbs distributions and the Bayesian restoration of images*. IEEE Transaction on Pattern Analysis and Machine Intelligence, 1984, **6**(6): 721–741.

[14] C. GOUT, C. LE GUYADER, L. A. VESE. *Segmentation under geometrical conditions with geodesic active contour and interpolation using level set methods*. Numerical Algorithms, 2005, **39**: 155–173.

[15] C. LE GUYADER, C. GOUT. *Geodesic active contour under geometrical conditions theory and 3D applications*. Numerical Algorithms, 2008, **48**: 105–133.

[16] S. HANOV. *Wavelets and edge detection*. University of Waterloo, Project report, 2006, http://stevehanov.ca/.

[17] Michael KASS, Andrew WITKIN, Demetri TERZOPOULOS. *Snakes: Active contour models*. International Journal of Computer Vision, 1988, **1**(4): 321–331.

[18] C. LI, C. XU, C. CUI, et al. *Level set evolution without re-initialization: A new variational formulation*. In Proceedings of IEEE Conference on Computer Vision and Pattern Recognition (CVPR'05), volume1, page 430–436, Washington, DC, USA, 2005. IEEE Computer Society.

[19] Chunming LI, Chiu-Yen KAO, J. C. GORE, et al. *Implicit active contours driven by local binary fitting energy*. In IEEE Conference on Computer Vision and Pattern Recognition (CVPR'07), 2007, 1–7.

[20] J. LIE, M. LYSAKER, X. C. TAI. *A binary level set model and some applications to Mumford-Shah image segmentation*. IEEE Transactions on Image Processing, 2006, **15**(5): 1171–1181.

[21] T. LU, P. NEITTAANMAKI, X. C. TAI. *A parallel splitting-up method for partial differential equations and its application to Navier-Stokes equations*. RAIRO Mathematical Modeling and Numerical Analysis, 1992, **26**(6): 673–708.

[22] J. MALIK, S. BELONGIE, T. LEUNG, et al. *Contour and texture analysis for image segmentation*. International Journal of Computer Vision, 2001, **43**: 7–27.

[23] R. MALLADI, J. A. SETHIAN. *A real-time algorithm for medical shape recovery*. In Proceedings of International Conference on Computer Vision, pages 304–310, Mumbai, India, 1998.

[24] Stephane MALLAT. *A Wavelet Tour of Signal Processing*. Academic Press, USA, 1998.

[25] P. MORROW, S. MCCLEAN, K. SAETZLE. *Contour detection of labelled cellular structures from serial ultrathin electron microscopy sections using GAC and prior analysis*. IEEE Proceedings of IPTA, 2008, 1–7.

[26] D. MUMFORD, J. SHAH. *Boundary detection by minimizing functionals*. In IEEE Conference on Computer Vision and Pattern Recognition, 1985.

[27] D. MUMFORD, J. SHAH. *Optimal approximations by piecewise smooth functions and associated variational problems*. Communications on Pure and Applied Mathematics, 1989, **42**: 577–685.

[28] Thi N. A. NGUYEN, Jianfei CAI, Juyong ZHANG, et al. *Robust interactive image segmentation using convex active contours*. IEEE Transactions on Image Processing, 2012, **21**(8), 3734-3743.

[29] Adam M. OBERMAN. *A convergent difference scheme for the infinity Laplacian: construction of absolutely minimizing Lipschitz extensions*. Math. Comp., 2005, **74**(251): 1217–1230.

[30] S. OSHER, J. A. SETHIAN. *Fronts propagating with curvature-dependent speed: algorithms based on Hamilton-Jacobi formulations*. J. Comput. Phys., 1988, **79**(1): 12–49.

[31] N. PARAGIOS, R. DERICHE. *Geodesic active contours and level sets for the detection and tracking of moving objects*. IEEE Transactions on Pattern Analysis and Machine Intelligence, 2000, **22**(3): 266–280.

[32] L. RADA, Ke CHEN. *A new variational model with dual level set functions for selective segmentation*. Commun. Comput. Phys., 2012, **12**(1): 261–283.

[33] D. SEN, S. K. PAL. *Histogram thresholding using fuzzy and rough measures of association error*. IEEE Transactions on Image Processing, 2009, **18**(4): 879–888.

[34] A. TSAI, A. J. YEZZI, A. S. WILLSKY. *Curve evolution implementation of the Mumford-Shah functional for image segmentation, denoising, interpolation, and magnification*. IEEE Transactions on Image Processing, 2001, **10**: 1169–1186.

[35] N. VALIAMMAL, S. N. GEETHALAKSHMI. *Performance analysis of various leaf boundary edge detection algorithms*. In Proceedings of the 1st Amrita ACM-W Celebration on Women in Computing in India, A2CWIC'10, pages 34:1–34:6, New York, USA, 2010, ACM.

[36] A. VASILEVSKIY, K. SIDDIQI. *Flux-maximizing geometric flows*. IEEE Transaction on Pattern Analysis and Machine Intelligence, 2002, **24**: 1565–1578.

[37] L. A. VESE, Tony F. CHAN. *A multiphase level set framework for image segmentation using the Mumford and Shah model*. International Journal of Computer Vision, 2002, **50**(3): 271–293.

[38] J. WEICKERT, G. KÜHNE. *Fast methods for implicit active contour*. In S. Osher and N. Paragios, editors, Geometric Level Set Methods in Imaging, Vision, and Graphics, pages 43–57, Springer, New York, 1995.

[39] J. WEICKERT, B. M. ROMENY, M. A. VIERGEVER. *Efficient and reliable schemes for nonlinear diffusion filtering*. IEEE Transactions on Image Processing, 1998, **7**(3): 398–410.

[40] J. P. ZHANG, Ke CHEN, Bo YU. *Local information based image selection segmentation model and fast robust algorithm*. Submitted, 2012.

[41] Kaihua ZHANG, Huihui SONG, Lei ZHANG. *Active contours driven by local image fitting energy*. Pattern Recognition, 2010, **43**(4): 1199–1206.

[42] Xiangrong ZHANG, Feng DONG, G. CLAPWORTHY, et al. *Semisupervised tissue segmentation of 3D brain MR images*. In 14th International Conference on Information Visualisation, 2010, 623–628.

[43] Guopu ZHU, Shuqun ZHANG, Qingshuang ZENG, et al. *Boundary-based image segmentation using binary level set method*. Opt. Engng., 2007, **46**(5): 050501 1–13.

[44] S. W. ZUCKER. *Region growing: childhood and adolescence*. Computer Graphics and Image Processing, 1976, **5**: 382–399.